DENSITY DIAGNOSTICS OF THE HOT PLASMA IN AE AQUARII WITH XMM-NEWTON

Manabu Ishida

Department of Physics, Tokyo Metropolitan University, 1-1 Minami-Osawa, Hachioji, Tokyo 192-0397, JAPAN

ABSTRACT

We report on *XMM-Newton* observations of the magnetic cataclysmic variable (mCV) AE Aqr. High resolution spectroscopy of the He-like triplet of N and O with the RGS has enabled us to measure the electron number density of the plasma to be $\sim 10^{11}$ cm^{-3}. Incorporating this with the emission measure, we estimate the geometrical scale of the plasma responsible for the N and O line emission, with ionization temperature $kT_i = 0.2-0.3$ keV, to be $\ell_{\rm p} \simeq (2\text{–}3) \times 10^{10}$ cm. Since both the density and the scale are incompatible with a standard post-shock accretion column of a mCV, the hot plasma in AE Aqr cannot be a product of mass accretion onto the white dwarf. The widths of the H-like Kα emission (= Lyα) lines of N and O, on the other hand, are measured to be $1250-1600$ km s^{-1} with the RGS. This is significantly larger than the thermal velocity expected for the ionization temperature of N and O plasma, but is rather consistent with that of the maximum plasma temperature $kT_{\rm max} = 4.6$ keV measured with the EPIC cameras. It is known that Balmer series and UV emission lines also show similar line widths. As the optical and UV lines, the X-ray emission lines also show dramatic flaring activity. These facts strongly suggest that all these broad emission lines from X-ray to optical wavebands are produced in the course of adiabatic cooling of the plasma once heated up to $T_{\rm max}$ in the deep gravitational potential of the white dwarf.

Key words: binaries: close — novae, cataclysmic variables — stars: individual (AE Aquarii) — plasmas — X-rays: stars.

1. INTRODUCTION

AE Aqr is a close binary system composed of a magnetized white dwarf rotating at a period of 33.08 s (Patterson, 1979) and a late type K3V-K5V star (Welsh, Horne, & Gomer, 1995) in a 9.88-h orbit (Welsh, Horne, & Gomer, 1993) whose inclination angle is $58^\circ \pm 6^\circ$ (Casares et al., 1996). The masses of the primary and the secondary are evaluated to be $M_1 = 0.79 \pm 0.16 M_\odot$ and $M_2 = 0.50 \pm 0.10 M_\odot$ (Casares et al., 1996).

AE Aqr has been known as one of the most enigmatic magnetic Cataclysmic Variables (mCVs) showing large optical flares and flickering (Patterson, 1979), large radio flares (Bastian, Beasley, & Bookbinder, 1996), TeV γ-ray emissions (Meintjes et al., 1994). In addition to these, although the long orbital period leads us to expect an accretion disk, the spectral profile of an Hα emission line is single-peaked and its centroid velocity is found to be inconsistent with the white dwarf orbit but lags behind the secondary orbit by some 70°–80° (Welsh, Horne, & Gomer, 1993). Spectral widths of Balmer emission lines are highly variable with a full width at zero intensity of $\sim$1000 km s^{-1} to over 4000 km s^{-1} during flares for the Hα line (Welsh, Horne, & Gomer, 1998). The widths of the same order are reported also for Hβ and Hγ emission lines (Reinsch & Beuermann, 1994). Hard X-ray emission from mCVs originates from the post-shock plasma in an accretion column whose temperature is a few tens of keV in mCVs in general (Ezuka & Ishida, 1999; Ishida & Fujimoto, 1995). The maximum temperature of AE Aqr is, on the other hand, as low as ~ 3 keV (Eracleous, 1999; Choi, Dotani, & Agrawal, 1999). All of these results, along with the discovery of a steady spin-down of the white dwarf at a rate $\dot{P} = 5.64 \times 10^{-14}$ s s^{-1} (de Jager et al., 1994), led Wynn, King, & Horne (1997) to introduce the magnetic propeller model in which "blobby" accreting matter originally following a ballistic trajectory from the inner Lagrangian point, experiences a drag from the magnetic field of the white dwarf, and is finally blown out of the binary due to so-called propeller action.

In this paper, we present results of density diagnostics of the plasma in AE Aqr by means of a well-resolved He-like triplet of N and O with the RGS. The results of this observation will be found in full detail in Itoh et al. (2006).

2. OBSERVATION

AE Aqr was observed with *XMM-Newton* on 2001 November 7–8. In total, 27 ks data are available for the

RGS and 17 ks for the EPIC pn/MOS. A detailed observation log can be found in Itoh et al. (2006). In Fig. 1 shown are the pn, MOS1, RGS1 and RGS2 light curves. As evident from the RGS2 light curve, the X-ray emis-

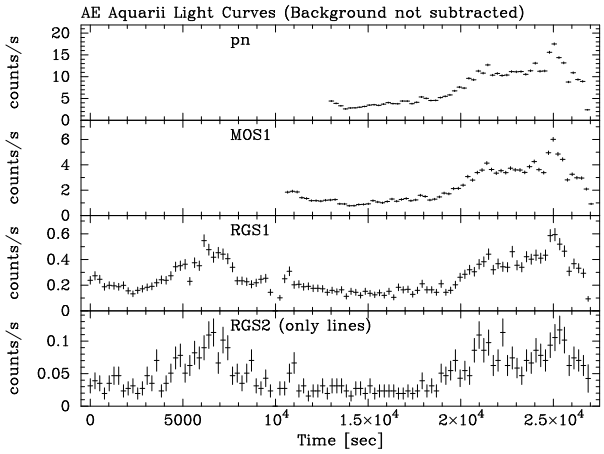

Figure 1. The light curves of EPIC pn and MOS1 in the band 0.2–15 keV, RGS1 in the band 5–35 Å, and RGS2 only with H-like and He-like Kα photons from N, O and Ne, but excluding the He-like Kα of O for which the corresponding CCD chip is dead. A common bin size of 256 sec is adopted. The source integration region is a circle with a radius of $57\farcs4$ and $50\farcs6$ for pn and MOS1, respectively. The RGS light curves are created with the 1st order photons.

sion lines show dramatic flaring activity as the optical and UV emission lines do (Eracleous & Horne, 1996), in correlation with the continuum emission that dominates the EPIC light curves and spectra.

We have searched for an X-ray pulsation in the EPIC pn light curve created in the band 0.2–10 keV, and have detected a sinusoidal pulse at a period of 33.08 ± 0.04 s by means of the epoch folding method both during quiescence and flare periods (time intervals of 13,000–18,700 s and 21,000–27,000 s in Fig. 1, respectively). The pulse period is consistent with the optical one (Patterson, 1979; de Jager et al., 1994).

3. DATA ANALYSIS

3.1. EPIC Spectra

The time-averaged energy spectrum extracted from the EPIC MOS2 is shown in Fig. 2. A number of H-like and/or He-like Kα emission lines of abundant metals from N through Fe can be recognized. The coexistence of these lines indicates that the X-ray-emitting plasma is optically thin and thermal, and has a significant temperature distribution in the range $kT \simeq$ 0.1–10 keV. In fact, we need four optically thin thermal plasma emission components with different temperatures to fit the spectra of the EPIC pn, MOS1, and MOS2 simultaneously. The

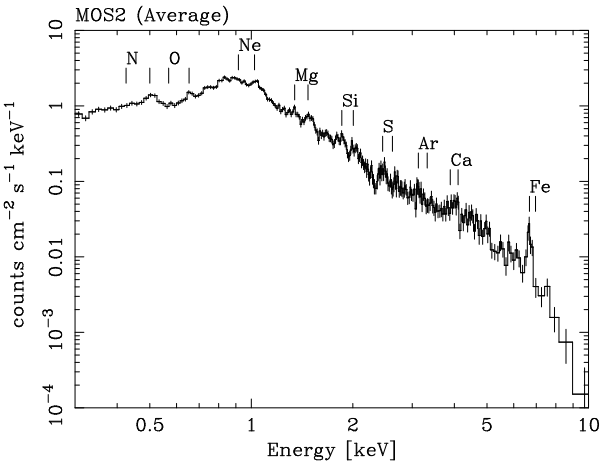

Figure 2. The time-averaged spectrum of AE Aqr taken with the EPIC MOS2. Energies of hydrogenic and He-like Kα lines from N through Fe are indicated with short vertical lines.

parameters of the best-fit 4-temperature VMEKAL model are summarized in table 1. The resultant temperatures are 0.14, 0.59, 1.4, and 4.6 keV. Their emission measures are 1.3, 3.6, 2.7, and $5.3 \times 10^{53}\mathrm{cm}^{-3}$, and in total $1.29 \times 10^{54}\mathrm{cm}^{-3}$, for an assumed distance of 100 pc (Welsh, Horne, & Oke, 1993; Friedjung, 1997). A common hydrogen column density of 3.6×10^{20} cm^{-2} is necessary to represent the photoelectric absorption. The metal abundances are subsolar and are in the range 0.4-$0.8Z_{\odot}$ in general, except for N, where $Z = 3.5 \pm 0.9Z_{\odot}$.

3.2. Spectra of He-like Triplets from the RGS

In Fig. 3 we have shown the RGS spectrum averaged throughout the observation. Kα emission lines from N through Si in the H-like and/or He-like ionization states can easily be recognized. Figure 4 (a)-(c) are blow-ups of energy bands of the He-like triplets of N, O, and Ne. In the next column (d)–(f) shown are the spectra predicted by the best-fit 4-temperature VMEKAL model. The intercombination line (i in the figure) is stronger and the forbidden (f in the figure) is weaker in the observed spectra, compared to the model spectra for N and O. This behavior can be attributed to a high density effect. If the electron density exceeds a certain critical value inherent in each element, on the other hand, one of the two electrons excited to the upper level of the forbidden line ($^3\mathrm{S}_1$) is further pumped to the higher level $^3\mathrm{P}_{2,1}$ by another impact of a free electron, and is then relaxed by radiating the intercombination line. The relative intensities of the intercombination and forbidden lines can therefore be utilized as a density diagnostic (Gabriel & Jordan, 1969; Pradhan & Shull, 1981; Porquet et al., 2001).

In order to obtain the electron number density n_{e}, we begin by evaluating intensities of the He-like triplets. For this, we utilize the 4-temperature VMEKAL model that provides the best-fit to the EPIC pn and MOS spectra

Table 1. The best-fit parameters of the 4 temperature vmekal model being fit to EPIC pn and MOS spectra

Parameter	Value	Element	Abundance[a]
$N_{\rm H}$ ($10^{20}{\rm cm}^{-2}$)	$3.59^{+1.47}_{-1.20}$	N	$3.51^{+0.92}_{-0.81}$
kT_1 (keV)	$4.60^{+0.60}_{-0.47}$	O	$0.74^{+0.17}_{-0.23}$
kT_2 (keV)	$1.21^{+0.13}_{-0.08}$	Ne	$0.43^{+0.28}_{-0.25}$
kT_3 (keV)	$0.59^{+0.02}_{-0.02}$	Mg	$0.70^{+0.15}_{-0.14}$
kT_4 (keV)	$0.14^{+0.05}_{-0.02}$	Si	$0.81^{+0.15}_{-0.12}$
$N_1^{\rm b}$ (10^{-3})	$4.45^{+0.41}_{-0.44}$	S	$0.73^{+0.20}_{-0.18}$
$N_2^{\rm b}$ (10^{-3})	$2.25^{+0.52}_{-0.51}$	Ar	$0.21\ (<0.89)$
$N_3^{\rm b}$ (10^{-3})	$3.04^{+0.47}_{-0.41}$	Ca	$0.19\ (<1.11)$
$N_4^{\rm b}$ (10^{-3})	$1.07^{+0.64}_{-0.37}$	Fe	$0.47^{+0.07}_{-0.06}$
$N_{\rm pn}/N_{\rm MOS}^{\rm c}$	$1.08^{+0.01}_{-0.01}$	Ni	$1.27^{+0.57}_{-0.50}$
χ^2_ν (d.o.f.)	1.22 (992)		

a: Solar Abundances (Anders & Grevesse, 1989)
b: Normalization of the VMEKAL component obtained with pn camera in a unit of $10^{-14}/4\pi D^2 \int n_e n_H\ dV$, where D [cm] is the distance to the target star.
c: Ratio of continuum normalizations.

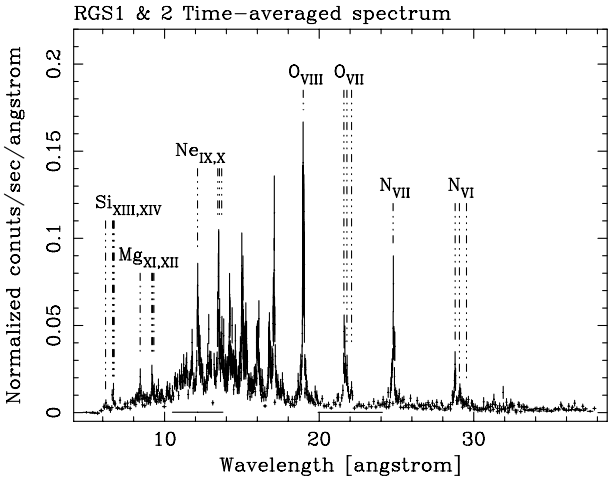

Figure 3. The averaged RGS spectra. Identifications of the H-line and He-like Kα lines of N through Si are shown with dotted-dashed line. The other unidentified lines are mainly those associated with Fe-L transitions.

(§ 3.1). The abundances are also fixed at the best-fit values, except for an element to be used as a density diagnostic, for which the abundance is set equal to zero, and instead, four Gaussians are added, representing the He-like triplet and the Lyα line. The best-fit model is displayed in Fig. 4 (a)-(c) as the histograms.

The ionization temperatures kT_i calculated from the intensity ratio between the Lyα and r are obtained to be 0.18, 0.30, and 0.34 keV for N, O, and Ne, respectively. The emission measures (EMs) of the plasma components with these temperatures can be calculated from the intensities of the Lyα and r lines with the aid of the EPIC abundances (see table 1), which result in EM =1.5, 1.8, and 9.1$\times 10^{53}$ cm^{-3}, respectively.

Given the line intensities of the triplets, we have carried out density diagnostics by means of the intensity ratio $f/(r+i)$. In Fig. 4 (g)-(i) shown are theoretical curves of the ratio $f/(r+i)$ versus the electron number density calculated with the plasma code SPEX (Kaastra, Mewe, & Nieuwenhuijzen, 1996) at kT_i of each element. In each panel we have also drawn a range of the intensity ratio allowed from the data and the resultant density range as a box. The electron number densities are found to be $(0.14$–$1.3) \times 10^{11}{\rm cm}^{-3}$, $(0.40$–$6.8) \times 10^{11}{\rm cm}^{-3}$, and $< 9.3 \times 10^{12}{\rm cm}^{-3}$ for N, O, and Ne, respectively. As an approximation, we obtain $n_{\rm e} \simeq 10^{11}{\rm cm}^{-3}$. This density, together with the emission measure obtained above, results in the linear scale of the plasma components with $kT_i = 0.2$–0.3 keV of $\ell_{\rm p} = (EM/n_{\rm e}^2)^{1/3} \simeq$ (2–3) $\times 10^{10}$ cm.

3.3. Spectra of H-like Kα Lines from the RGS

It is known that the wavelength of the Hα line from AE Aqr shows a sinusoidal orbital Doppler modulation with an amplitude of $\sim$150 km s^{-1} (Robinson, Shafter, & Balachandran, 1991; Wynn, King, & Horne, 1997; Welsh, Horne, & Gomer, 1998). A similar behavior is found from a series of UV emission lines with a velocity amplitude of generally 110–220 km s^{-1} (Eracleous & Horne, 1996). In order to search the X-ray emission lines for a similar orbital modulation, we have made RGS spectra during the first and second flares separately. The spectra are accumulated during time intervals of 3,000–8,500 s and 19,000–26,000 s in Fig. 1 for the two flares. The corresponding orbital phases are $\phi = 0.81$–0.93 and $\phi = 0.29$–0.46, respectively. We have evaluated profiles of spectrally isolated H-like Kα lines (= Lyα lines) from N and O by fitting a Gaussian to them. Unfortunately, the line central energies are consistent with those in the laboratory, and any systematic orbital motion of the line-emitting gas is not detected.

Note, however, that the 1σ line width $\Delta E_{{\rm Ly}\alpha}$ is found to be $\simeq$ 1.2 eV and $\simeq$ 2 eV for the N and O Lyα lines on average, which corresponds to a line-of-sight velocity dispersion $<v_1>$ (= $(\Delta E_{{\rm Ly}\alpha}/E_{{\rm Ly}\alpha})\,c$) of $\simeq$720 km s^{-1} and $\simeq$920 km s^{-1}, respectively. These values are much larger than the thermal velocity, e.g., ~ 0.16 eV or $\sim$ 70 km s^{-1} for oxygen, estimated from $kT_i = 0.3$ keV. Note also that the line-of-sight orbital velocity amplitude is $\simeq \frac{M_1}{M_1+M_2}\,\frac{2\pi}{P_{\rm orb}}\,a\cos i \simeq 100$ km s^{-1}, which is also small enough.

4. DISCUSSION

4.1. Implication of the Low Plasma Density

The electron number density of the plasma measured from the He-like triplets of N and O ($\simeq 10^{11}{\rm cm}^{-3}$) is smaller by several orders of magnitude than the con-

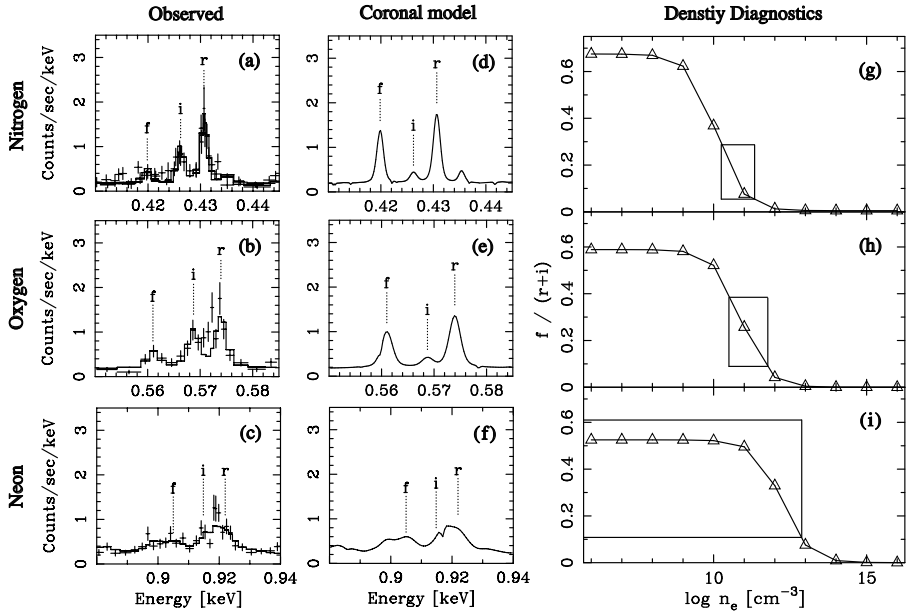

Figure 4. Density diagnostics by means of the He-like triplet. Panels of observed and coronal limit spectra around the He-like triplet, and the density diagnostics are arranged from left to right columns. The cases of Nitrogen, Oxygen, and Neon are arranged from upper to lower raws. The relative intensities of the intercombination (marked with 'i') and forbidden (marked with 'f') lines are undoubtedly inverted for N and O. Panels (g)-(i) compare theoretical curves of the intensity ratio $f/(r+i)$ as a function of $n_{\rm e}$ with the observed intensity ratio. In drawing the theoretical curves we have used the plasma code SPEX *(Kaastra, Mewe, & Nieuwenhuijzen, 1996) at the ionization temperatures kT_i of 0.18, 0.30, and 0.34 keV for N, O, and Ne obtained from the intensity ratio between Lyα and r.*

ventional estimate in the post-shock accretion column of mCVs, $n_{\rm e} \simeq 10^{16}$ cm^{-3} (Frank, King, & Raine, 2002). Moreover, the resultant scale ($\ell_{\rm p} = (2-3) \times 10^{10}$ cm) is larger than the radius of the white dwarf (assumed to be $\sim 7 \times 10^8$ cm for a $0.79 M_\odot$ white dwarf) by more than an order of magnitude, and is rather a fraction of the size of the Roche lobe of the primary. We thus conclude that, unlike other mCVs, the X-ray-emitting plasma in AE Aqr is not a product of the mass accretion onto the white dwarf.

We would like to remark here that photo-excitation due to UV radiation can also pump a $^3{\rm S}_1$ electron up into the $^3{\rm P}_{2,\,1}$ level, thereby affecting the density diagnostics (Gabriel & Jordan, 1969; Pradhan & Shull, 1981; Porquet et al., 2001). Since there is no evidence of an accretion disk in AE Aqr (Welsh, Horne, & Gomer, 1993), and the secondary is a late type K3-K5 star, the hot polarcap region of the white dwarf, occupying 0.6 % of the surface area emitting with a 47,000 K blackbody spectrum (Eracleous & Horne, 1996), is the most efficient UV-radiation source. With this emission, however, the photo-excitation rate is only $\sim$0.2 % of the collisional-excitation rate, and hence, can be neglected (Itoh et al., 2006).

4.2. Plasma Heating and Propeller Condition

From the *XMM-Newton* observations, we have obtained the maximum temperature of the plasma $kT_{\rm max}$ to be 4.6 keV (table 1). This implies the matter transferred from the secondary star is accelerated at least to the corresponding thermal velocity $v_{\rm th} = (3kT_{\rm max}/\mu m_{\rm H})^{1/2} \simeq 1500$ km s^{-1}. Such a high velocity can naturally be achieved by utilizing the gravitational potential of the white dwarf. Theoretical model calculations of the Doppler tomograms by Wynn, King, & Horne (1997) and Welsh, Horne, & Gomer (1998) also predict that the high velocity can be realized only within the Roche lobe of the white dwarf. We thus assume, as in Choi, Dotani, & Agrawal (1999), that the observed maximum temperature is attributed to the release of the gravitational energy. We can then make an order of magnitude estimate of the radius $r_{\rm th}$ where such thermalization takes place from

$$\frac{3}{2}\, kT_{\rm max} \;\sim\; \frac{GM_1}{r_{\rm th}}\, \mu m_{\rm H}, \qquad (1)$$

which results in $r_{\rm th} \sim 1 \times 10^{10}$ cm. This number is roughly of the same order as the theoretical minimum distance estimates of blobs $r_{\rm min} > 10^{10}$ cm by Wynn, King, & Horne (1997). At $r_{\rm th}$, the corotation velocity $v_{\rm co} = 1.9 \times 10^9$ cm s^{-1} is much larger than the local Kepler velocity $v_{\rm K} = 1.0 \times 10^8$ cm s^{-1}. Hence, the plasma heated at $r \sim r_{\rm th}$ is possible to be expelled due to the magnetic propeller action by the white dwarf.

4.3. Implications of the Broad H-like Kα Lines

As presented in § 3.3, the observed spectral widths of the Lyα lines result in a line-of-sight velocity dispersion

$< v_1 >$ of $\simeq$720 km s^{-1} and $\simeq$920 km s^{-1} for N and O, respectively. These values are much larger than that expected from the thermal broadening (§ 3.3). It is interesting to note that the three-dimensional velocity dispersion $< v_3 >$ of 1250$-$1600 km s^{-1} ($= \sqrt{3} < v_1 >$) is comparable to the thermal velocity of the plasma $v_{\rm th} = (3kT_{\rm max}/\mu m_{\rm H})^{1/2} = 1500$ km s^{-1} where $kT_{\rm max} = 4.6$ keV (§ 3.1). The plasma of the N and O emission ($kT_i = 0.2-0.3$ keV) can thus be regarded as having been cooled through adiabatic expansion of the seed blob which is once heated up to $T_{\rm max}$ in the deep gravitational potential of the white dwarf. This scenario is supported by the fact that the expansion times scale $t_{\rm exp} = \frac{\ell_{\rm p}}{v_{\rm th}} \simeq 100$ s is much shorter than the radiative cooling time scale of the plasma $t_{\rm cool} = \frac{3n_{\rm e}kT_{\rm e}V}{L_{\rm X}} \simeq 4.8 \times 10^3$ s (Itoh et al., 2006). Theoretically, Wynn, King, & Horne (1997) estimated the density and the size of the original blob to be 10^{13}–10^{14} cm^{-3} and 10^9 cm. By comparing these numbers with our estimates $n_{\rm e} \sim 10^{11}$ cm^{-3} and $\ell_{\rm p} = (2-3) \times 10^{10}$ cm (§ 3.2), we conclude that the plasma of the N and O emission can be interpreted as a result of the adiabatic expansion of the blob.

The observed N and O Lyα line width of $< v_1 > = 720-920$ km s^{-1} is reminiscent of that of the Balmer series and UV emission lines. During optical flares, the spectral width of Hβ and Hγ lines increases up to a full width at half maximum (FWHM) of $\sim$25Å (Reinsch & Beuermann, 1994). Dividing the FWHM by a factor of 2.355, we obtain $< v_1 >$=650$-$730 km s^{-1} for the Hβ and Hγ. Welsh, Horne, & Gomer (1998) have obtained a full width at zero intensity of Hα emission line during optical flares to be $\sim$4000 km s^{-1}. Assuming the corresponding FWHM roughly to be $\sim$2000 km s^{-1}, we obtain $< v_1 > \sim$ 850 km s^{-1}. Eracleous & Horne (1996) have estimated a FWHM of the He 2 line (λ1640) to be 1700 km s^{-1}, equivalent to $< v_1 > \simeq$ 720 km s^{-1}. The common observed spectral width of all these X-ray to optical emission lines strongly suggests that the plasmas responsible for these lines are all descendants of the blob once being heated up to $T_{\rm max}$ and then being cooled through adiabatic expansion. The observed X-ray to optical broad lines can be considered as being emitted in the course of this cooling process. As the optical and UV emission lines, the X-ray emission lines also show dramatic flaring activity, as shown in Fig. 1. This also supports the picture that all the emission lines have common origin.

The picture presented here can provide a solution to one of the problems (Welsh, 1999) in the original propeller model, the absence of the theoretically-predicted high velocity loop component (Wynn, King, & Horne, 1997) in the observed Hα tomogram, which leads Welsh, Horne, & Gomer (1998) to introduce the colliding-blob model. This model intends to limit the Hα emission location out of the Roche lobe of the primary by introducing distributions for the density and the size of the blobs. Our results, on the other hand, suppress the high velocity component of the Hα emission line without any additional assumption in the way that the propelled plasma is still too hot ($kT_i = 0.2-0.3$ keV) to emit Hα lines within a radius of $\sim \ell_{\rm p}$ ($\simeq$ the Roche lobe size) from the white dwarf, where the high velocity component is expected to originate.

5. CONCLUSION

We have presented the results from *XMM-Newton* observations of AE Aqr carried out on 2001 November 7-8. Owing to the high energy-resolving power of the RGS, the intensity ratio of the intercombination to forbidden lines of the He-like triplet from nitrogen and oxygen is found to be larger than that expected for the plasma in the low-density limit, which has enabled us to measure the electron number density to be $\sim 10^{11}$ cm^{-3}. This, together with the emission measure ($\simeq 10^{53}$–10^{54} cm^{-3}), results in a geometrical scale $\ell_{\rm p}$ of the plasma of the N and O line emissions, with the ionization temperature $kT_{\rm i}$ of 0.2–0.3 keV, to be $\simeq$ (2–3) $\times 10^{10}$ cm. The density is smaller than that of a standard post-shock plasma of mCVs by several orders of magnitude, and $\ell_{\rm p}$ is much larger than the radius of a $0.79 M_\odot$ white dwarf. We thus conclude that the X-ray-emitting plasma in AE Aqr cannot be a product of mass accretion onto the white dwarf.

Average spectra of the EPIC cameras can be reproduced by a four-temperature optically thin thermal plasma emission model with a maximum temperature $kT_{\rm max}$ of 4.6 keV. Assuming this temperature is achieved by converting gravitational potential energy into heat, we have made an order of magnitude estimate of the radius for the heating to occur as $r_{\rm th} \sim 1 \times 10^{10}$ cm. As the corotation velocity with the white dwarf at $r_{\rm th}$ is much larger than the Keplerian velocity, the resultant hot plasma can be expelled due to the magnetic propeller action by the white dwarf.

RGS spectroscopy of H-like Kα emission (= Lyα) lines of N and O has revealed that they show a significant broadening with a 1-σ width of $\sim$1.2 eV and $\sim$2 eV, respectively, corresponding to a line-of-sight velocity dispersion $< v_1 >$ of 720–920 km s^{-1}. Since the velocity dispersion $< v_3 >= 1250$–1600 km s^{-1} ($= \sqrt{3} < v_1 >$) is comparable to the thermal velocity of the plasma with $kT_{\rm max} = 4.6$ keV ($v_{\rm th} = (3kT_{\rm max}/\mu m_{\rm H})^{1/2} = 1500$ km s^{-1}), the plasma producing the N and O emission lines ($kT_i = 0.2-0.3$ keV) can be interpreted as having expanded adiabatically since it is heated up to $T_{\rm max}$ in the deep gravitational potential of the white dwarf. It is interesting to note that the Balmer series and UV emission lines also show a spectral width with a similar $< v_1 >$ of 650$-$850 km s^{-1}. This strongly suggests that all these broad emission lines from X-ray to optical wavebands emanate from the plasma, which is once heated up to $T_{\rm max}$ at $r_{\rm th}$, in the course of its adiabatic cooling. The dramatic flaring activity of the X-ray emission lines, along with the optical and UV lines, require a common origin for all these lines. The picture presented here can explain the absence of the high velocity component of the Hα emission line in the way that the plasma expelled due to the propeller action is still too hot

($kT_i = 0.2-0.3$ keV) to emit the Hα line within a region of $r < \ell_{\rm p}$ ($\simeq$ the Roche lobe size) from the white dwarf where the high velocity component is expected to originate.

REFERENCES

Anders, E. & Grevesse, N. 1989, Geochim. Cosmochim. Acta, 53, 197

Bastian, T. S., Beasley, A. J., & Bookbinder, J. A. 1996, ApJ, 461, 1016

Casares, J., Mouchet, M., Martinez-Pais, I. G., & Harlaftis, E. T. 1996, MNRAS, 282, 182

Choi, C., Dotani, T., & Agrawal, P. C. 1999, ApJ, 525, 399

de Jager, O. C., Meintjes, P. J., O'Donoghue, D., & Robinson, E. L. 1994, MNRAS, 267, 577

Eracleous, M. 1999, ASP Conf. Ser. 157: Annapolis Workshop on Magnetic Cataclysmic Variables, 343

Eracleous, M., & Horne, K. 1996, ApJ, 471, 427

Ezuka, H. & Ishida, M. 1999, ApJS, 120, 277

Frank, J., King, A., & Raine, D. J. 2002, Accretion Power in Astrophysics: Third Edition, by Juhan Frank, Andrew King, and Derek J. Raine. Cambridge University Press, 2002, 398 pp., Chapter 6

Friedjung, M. 1997, New Astronomy, 2, 319

Gabriel, A. H. & Jordan, C. 1969, MNRAS, 145, 241

Ishida, M. & Fujimoto, R. 1995, ASSL Vol. 205: Cataclysmic Variables, 93

Itoh, K., Okada, S., Ishida, M., & Kunieda, H. 2006, ApJ, to appear in vol. 639 March 01 issue.

Kaastra, J. S., Mewe, R., & Nieuwenhuijzen, H. 1996, UV and X-ray Spectroscopy of Astrophysical and Laboratory Plasmas : Proceedings of the Eleventh Colloquium on UV and X-ray ... held on May 29-June 2, 1995, Nagoya, Japan. Edited by K. Yamashita and T. Watanabe. Tokyo : Universal Academy Press, 1996. (Frontiers science series ; no. 15)., p.411

Meintjes, P. J., de Jager, O. C., Raubenheimer, B. C., Nel, H. I., North, A. R., Buckley, D. A. H., & Koen, C. 1994, ApJ, 434, 292

Patterson, J. 1979, ApJ, 234, 978

Porquet, D., Mewe, R., Dubau, J., Raassen, A. J. J., & Kaastra, J. S. 2001, A&A, 376, 1113

Pradhan, A. K. & Shull, J. M. 1981, ApJ, 249, 821

Reinsch, K., & Beuermann, K. 1994, A&A, 282, 493

Robinson, E. L., Shafter, A. W., & Balachandran, S. 1991, ApJ, 374, 298

Welsh, W. F. 1999, ASP Conf. Ser. 157: Annapolis Workshop on Magnetic Cataclysmic Variables, 357

Welsh, W. F., Horne, K., & Gomer, R. 1998, MNRAS, 298, 285

Welsh, W. F., Horne, K., & Gomer, R. 1995, MNRAS, 275, 649

Welsh, W. F., Horne, K., & Gomer, R. 1993, ApJ, 410, L39

Welsh, W. F., Horne, K., & Oke, J. B. 1993, ApJ, 406, 229

Wynn, G. A., King, A. R., & Horne, K. 1997, MNRAS, 286, 436